

Effective Sparsity: A Unified Framework via Normalized Entropy and the Effective Number of Nonzeros

Haoyu He

*School of Information Science and Technology
ShanghaiTech University
Shanghai, 201210, China*

HEHY12024@SHANGHAITECH.EDU.CN

Hao Wang*

*School of Information Science and Technology
ShanghaiTech University
Shanghai, 201210, China*

HAW309@GMAIL.COM

Jiashan Wang

*Department of Mathematics
University of Washington, USA*

JSW1119@GMAIL.COM

Hao Zeng

*School of Information Science and Technology
ShanghaiTech University
Shanghai, 201210, China*

ZENGHAO.HAOZENG@GMAIL.COM

Editor: My editor

Abstract

Classical sparsity-promoting methods rely on the ℓ_0 norm, which treats all nonzero components as equally significant. In practical inverse problems, however, solutions often exhibit numerous small-amplitude components that minimally affect reconstruction but lead to an over-estimation of the signal's complexity. We address this limitation by shifting the paradigm from discrete cardinality to effective sparsity. Central to our approach is the introduction of the effective number of nonzeros (ENZ), a unified class of normalized entropy-based regularizers—including Shannon and Rényi forms—that robustly quantifies the concentration of significant coefficients. We show that while the classical ℓ_0 norm is brittle, the ENZ provides a stable and continuous measure of effective sparsity that is invariant to negligible perturbations. For noisy linear inverse problems, we establish theoretical guarantees under the Restricted Isometry Property (RIP), proving that ENZ-based recovery is both unique and stable. Furthermore, we derive a fundamental decomposition that identifies the ENZ as a product of the support cardinality and a distributional efficiency term, explicitly bridging entropy with ℓ_0 regularization. Numerical experiments demonstrate that our effective sparsity framework significantly outperforms traditional cardinality-based methods in both robustness and accuracy.

Keywords: Effective Sparsity, Effective Number of Nonzeros (ENZ), Normalized Entropy, ℓ_0 Minimization, Inverse Problems, Restricted Isometry Property.

1 Introduction

Recovering sparse signals from underdetermined linear systems is a cornerstone problem in machine learning, high-dimensional statistics, and signal processing. Consider

$$A\mathbf{x} = \mathbf{b} + \boldsymbol{\varepsilon}, \quad (1.1)$$

where $A \in \mathbb{R}^{m \times n}$ is the sensing matrix with $m \ll n$, $\mathbf{b} \in \mathbb{R}^m$ represents the observed data, and $\boldsymbol{\varepsilon} \in \mathbb{R}^m$ denotes additive noise. Under the assumption that the true signal \mathbf{x} is sparse, the objective is to recover \mathbf{x} from limited measurements. This paradigm has driven significant advancements across a wide spectrum of applications, from compressed sensing to high-dimensional inference [Blumensath and Davies \(2008\)](#); [Candes et al. \(2006\)](#); [Chen et al. \(2001\)](#); [Donoho \(2006\)](#); [Fan and Li \(2001\)](#); [Tibshirani \(1996\)](#). However, most classical methods rely on a strict sparsity assumption, utilizing cardinality-based measures like the ℓ_0 norm that treat all nonzero entries as equally important. In practice, signals often exhibit effective sparsity, where the primary information is concentrated on a few dominant coefficients, while a “long tail” of small-amplitude components—often arising from noise or modeling fluctuations—drastically inflates the discrete cardinality without reflecting the signal’s true underlying complexity.

Traditionally, sparsity is quantified by the ℓ_0 “norm,” which counts the number of non-zero entries in a vector, leading to the combinatorial optimization problem [Blumensath and Davies \(2008\)](#):

$$\min_{\mathbf{x}} \|\mathbf{x}\|_0 \quad \text{subject to} \quad A\mathbf{x} = \mathbf{b}. \quad (1.2)$$

However, the ℓ_0 minimization problem is known to be NP-hard and exhibits extreme sensitivity to noise [Natarajan \(1995\)](#). To bridge the gap between theoretical ideals and computational feasibility, various surrogates have been developed, ranging from the convex ℓ_1 relaxation [Beck and Teboulle \(2009\)](#); [Tibshirani \(1996\)](#); [Chen et al. \(2001\)](#); [Candès et al. \(2006, 2008\)](#) to non-convex penalties such as ℓ_p ($0 < p < 1$) [Chartrand and Staneva \(2008\)](#), $\ell_1 - \ell_2$ [Yin et al. \(2015\)](#), and the scale-invariant ℓ_1/ℓ_2 ratio [Rahimi et al. \(2019\)](#); [Xu et al. \(2021\)](#). While these methods have achieved notable empirical successes, their theoretical guarantees often rely on the Restricted Isometry Property (RIP), where recovery conditions remain strictly tied to the literal cardinality of the signal’s support [Candès \(2008\)](#); [Blanchard et al. \(2011\)](#).

The Practical Mismatch of ℓ_0 Sparsity

Despite significant progress in sparse recovery, a fundamental discrepancy persists between ℓ_0 sparsity and the nature of signals encountered in realistic, noisy environments. In practice, solutions to $A\mathbf{x} = \mathbf{b}$ often contain a long tail of numerically small but non-zero components, stemming from numerical precision limits, modeling inaccuracies, or ambient noise [Lopes \(2013\)](#). While these components contribute negligibly to the signal’s energy or physical interpretation, they indiscriminately inflate the ℓ_0 count. This tension is particularly acute in compressed sensing theory. Classical recovery results typically ensure stability under a $2k$ -Restricted Isometry Property (RIP) condition, provided the signal contains k non-zero entries [Candes et al. \(2006\)](#); [Foucart and Rauhut \(2013\)](#). However, when infinitesimal perturbations are treated as genuine non-zeros, the apparent sparsity level k can increase

dramatically, forcing the RIP to hold at much higher orders. This leads to a theoretical paradox: the theoretical analysis imposes unnecessarily stringent measurement requirements primarily to capture negligible components, even when the meaningful structure of the signal remains unchanged. Consequently, theoretical guarantees based on ℓ_0 norm become overly pessimistic, demanding high sampling rates to protect entries that are essentially irrelevant. This observation suggests that cardinality alone is not the appropriate notion of sparsity in noisy inverse problems.

Effective Sparsity and Effective Non-zeros

Building on these limitations, we argue that a robust measure should capture effective sparsity—the number of components that meaningfully influence the signal’s structure Hill (1973); Roy and Vetterli (2007). Entropy, a fundamental concept in information theory, provides a natural and principled framework for this task Shannon (1948); Cover (1999); Jaynes (1957). Unlike cardinality, which is a binary property of the support, entropy-based measures reflect the continuous distribution of energy: low entropy corresponds to signals dominated by a few significant components, whereas high entropy indicates diffuse or noise-dominated structures.

In contrast to traditional magnitude-based penalties, we propose characterizing signal complexity in terms of the effective number of nonzeros (ENZ). The ENZ is an entropy-induced metric that prioritizes components which meaningfully contribute to the signal’s mass, rather than those that are merely non-zero in a literal sense. This robustness is essential in practical inverse problems, where numerical noise and modeling errors are unavoidable. By bridging entropy regularization with traditional sparse models, we clarify how distributional concentration serves as a stable proxy for cardinality.

Contribution

In this paper, we revisit sparse signal recovery by shifting the perspective from discrete support cardinality to effective sparsity. We argue that in practical, noisy environments, the conventional ℓ_0 norm serves as an overly pessimistic metric, as it fails to distinguish between primary signal components and negligible perturbations.

To address this, we propose an entropy-based view of sparsity, encompassing Shannon and Rényi Shannon (1948); Rényi (1961). By treating sparsity as a property of informational concentration rather than magnitude shrinkage, our framework introduces the ENZ—a robust metric that characterizes the informative core of a signal. Through a fundamental decomposition theorem and RIP-based stability analysis, we provide both the geometric intuition and the theoretical rigor necessary to bridge the gap between information theory and high-dimensional recovery. The principal contributions of this work are summarized as follows:

- **A Robust Measure of Effective Sparsity:** We formalize the concept of ENZ to quantify signal complexity. Unlike the brittle ℓ_0 norm, we prove that our entropy-induced metrics are continuous and stable under small-amplitude perturbations, providing a faithful characterization of a signal’s meaningful support.

- **De-coupled RIP Requirements and Stability:** For noisy linear inverse problems, we establish uniqueness and stability guarantees expressed directly in terms of effective sparsity. Our analysis demonstrates that entropy-based formulations yield significantly milder Restricted Isometry Property (RIP) requirements compared to classical ℓ_0 -based results.
- **A Unified Entropy-Based Sparsity Framework:** We introduce a general information-theoretic framework in which sparsity is quantified via entropy of the normalized coefficient magnitudes and enforced through corresponding (un)normalized entropy regularizers. This framework yields both scale-invariant effective sparsity indices (ENZ) and practical regularization functions with a consistent geometric and information-theoretic interpretation. Classical scale-invariant penalties, such as the ℓ_1/ℓ_2 ratio, appear as simple transforms of specific Rényi-based ENZ measures, illustrating how existing methods fit naturally into our entropy-based view of sparsity.
- **Geometric Decomposition Theorem:** We derive a decomposition theorem revealing that normalized entropy regularizers factor exactly into an ℓ_0 -type cardinality term and a divergence from uniformity over the active support. This decomposition provides a novel geometric interpretation: entropy minimization promotes sparsity by simultaneously reducing support size and maximizing energy concentration.

1.1 Outline

This paper is structured as follows. Section 2 introduces the basic concepts of entropy regularization and reviews relevant information-theoretic metrics. Section 3 defines the notion of effective number of nonzeros and Section 4 establishes its stability guarantees under the RIP. Section 5 presents decomposition theorems for normalized entropy regularizers, revealing how they separate sparsity from distributional imbalance. Section 7 provides numerical experiments validating the theoretical findings and comparing the performance of different entropy-based regularizers. Finally, Section 8 concludes the paper and discusses potential extensions.

1.2 Notation and Preliminaries

We denote $\mathbb{R}_+ = [0, \infty)$ and $\mathbb{R}_+^n = \{\mathbf{x} \in \mathbb{R}^n : x_i \geq 0, \forall i\}$. The $(n - 1)$ -dimensional probability simplex is defined as

$$\Delta^{n-1} = \left\{ \boldsymbol{\pi} = (\pi_1, \dots, \pi_n) \in \mathbb{R}_+^n : \sum_{i=1}^n \pi_i = 1, \pi_i \geq 0 \right\}.$$

The ℓ_p -norm of $\mathbf{x} = (x_1, \dots, x_n) \in \mathbb{R}^n$ is defined as $\|\mathbf{x}\|_p = (\sum_{i=1}^n |x_i|^p)^{1/p}$. The support of \mathbf{x} is $\text{Supp}(\mathbf{x}) := \{i : x_i \neq 0\}$, and its cardinality is denoted by $\|\mathbf{x}\|_0 = |\text{Supp}(\mathbf{x})|$.

For a probability distribution $\boldsymbol{\pi} \in \Delta^{n-1}$, we define:

- *Shannon entropy* Shannon (1948): $H(\boldsymbol{\pi}) = -\sum_{i=1}^n \pi_i \log_2 \pi_i$, with the convention $0 \log_2 0 = 0$.

- *Rényi entropy* (order $\alpha > 0, \alpha \neq 1$) Rényi (1961): $R_\alpha(\boldsymbol{\pi}) = \frac{1}{1-\alpha} \log_2(\sum_{i=1}^n \pi_i^\alpha)$, note that as $\alpha \rightarrow 1, R_\alpha(\boldsymbol{\pi}) \rightarrow H(\boldsymbol{\pi})$.
- *Kullback–Leibler (KL) divergence* between $\mathbf{p}, \mathbf{q} \in \Delta^{n-1}$ Kullback and Leibler (1951): $D_{\text{KL}}(\mathbf{p} \parallel \mathbf{q}) = \sum_{i=1}^n p_i \log_2 \frac{p_i}{q_i}$, with the conventions $0 \log_2(0/0) = 0$ and $p_i \log_2(p_i/0) = +\infty$ if $p_i > 0$.

2 The Effective Sparsity of Complex Systems

To rigorously characterize the complexity of real-world systems, it is essential to distinguish between the strict mathematical support of a signal and its effective information content. Intuitively, a vector \mathbf{x} is considered effectively sparse if its energy or magnitude is highly concentrated on a small subset of components, leaving the remaining entries nonzero but negligible in their contribution to the overall system behavior. While the classical sparsity measure $\|\mathbf{x}\|_0$ is typically full-dimensional in practice due to pervasive noise and modeling errors, the functional dynamics of high-dimensional systems are often governed by a much smaller set of dominant coordinates.

We quantify this phenomenon through the concept of effective sparsity, defined as the effective number of nonzeros: $\text{ENZ}(\mathbf{x}) = 2^{\mathcal{H}(\mathbf{x})}$. Unlike the discrete ℓ_0 norm, which treats all nonzero entries as equally significant, this entropy-based measure provides a continuous, magnitude-aware assessment of dimensionality. By satisfying $\text{ENZ}(\mathbf{x}) \ll n$, this metric bridges the gap between theory and practice: it captures the true number of active degrees of freedom while remaining robust to the “long tail” of negligible components that inflate the classical support without contributing to the system’s meaningful energy.

In this section, we present empirical evidence demonstrating that for representative high-dimensional datasets, the effective support governing system behavior is substantially smaller than the ambient dimension suggested by raw measurements. These findings highlight a distinct gap between the apparent complexity of the data and the functional degrees of freedom that actually determine the system’s state.

2.1 Evidence Supporting the Effective Sparsity

In this session, we will use real-world image and text datasets to demonstrate the prevalence of effectiveness sparsity in practical applications.

Effective Sparsity in Natural Images

We analyze natural images from both transform-domain and spatial-structure perspectives.

Wavelet-domain coefficient decay. We first examine the decay behavior of wavelet coefficients in natural images. A benchmark image set in Matlab (including *cameraman*, *peppers*, and related standard test images) is analyzed by decomposing each image using a Daubechies-4 (db4) wavelet basis with four levels of decomposition. For color images, the analysis is performed independently on each channel. All wavelet coefficients are normalized by their maximum absolute value, sorted in descending order, and plotted on a logarithmic scale against the normalized coefficient index. Figure 1 overlays decay curves from all images and reports summary statistics, including the mean, median, and percentile envelopes.

The results reveal a consistent and rapid decay pattern across the dataset. While the majority of coefficients are nonzero, their magnitudes decay rapidly, indicating that image content is not strictly sparse in the ℓ_0 sense but exhibits strong effective sparsity. Only a small fraction of coefficients captures the dominant energy and semantic structure, while the remaining coefficients form a dense but negligible tail. For readability, we summarize the decay behavior using percentile curves (rather than plotting every individual decay curve).

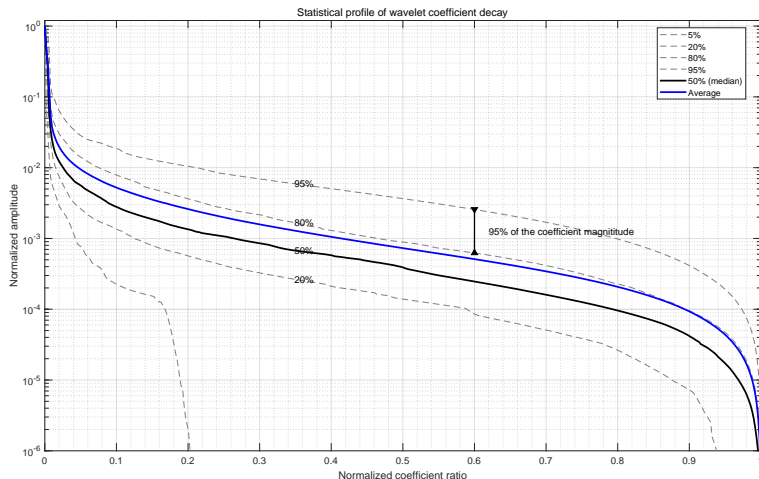


Figure 1: Effective sparsity in natural images. Sorted magnitude decay of wavelet coefficients for a collection of standard test images (including cameraman, peppers, and related benchmarks). Both grayscale images and individual color channels (RGB) are analyzed. Each image is normalized by its maximum pixel value and transformed using a Daubechies-4 (db4) wavelet basis with four decomposition levels. Coefficient magnitudes are sorted in descending order and normalized by their maximum value. Thin curves show individual decay profiles across images and channels. The blue solid curve denotes the mean decay, and the black solid curve denotes the median. Dashed curves indicate the 5%, 25%, 80%, and 95% percentile envelopes. The horizontal axis represents the normalized coefficient index (from largest to smallest), and the vertical axis shows the normalized coefficient magnitude on a logarithmic scale. The rapid decay demonstrates that natural images are not strictly sparse but exhibit pronounced effective sparsity, with most coefficients being nonzero yet negligible in magnitude.

Directional total variation decay. We further analyze spatial variation directly via total variation (TV). For each image $I \in \mathbb{R}^{m \times n}$, we define the forward finite differences

$$(D_x I)_{i,j} = I_{i,j+1} - I_{i,j}, \quad (D_y I)_{i,j} = I_{i+1,j} - I_{i,j}.$$

The discrete gradient at pixel (i, j) is

$$\nabla I_{i,j} = \begin{pmatrix} (D_x I)_{i,j} \\ (D_y I)_{i,j} \end{pmatrix}.$$

The anisotropic TV of I is defined as

$$\text{TV}(I) = \sum_{i,j} (|(D_x I)_{i,j}| + |(D_y I)_{i,j}|) = \|\nabla I\|_1.$$

To investigate sparsity in the TV sense, we collect the gradient magnitudes $|(D_x I)_{i,j}|$ and $|(D_y I)_{i,j}|$, normalize them by their maximum absolute value, and sort them in descending order. Figure 2 shows the resulting decay curves. The results show that both horizontal and vertical total variation components exhibit nearly identical decay behavior, characterized by rapid, approximately exponential attenuation.

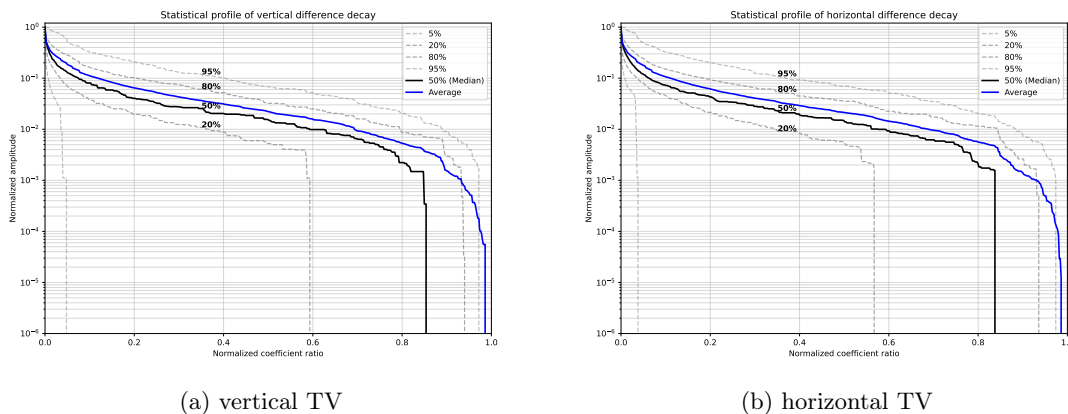


Figure 2: Effective sparsity in spatial variation of natural images. Sorted magnitude decay of directional total variation (TV) coefficients for the same collection of standard test images as in Figure 1. Horizontal (TV_x) and vertical (TV_y) finite differences are computed for each image; for color images, TV is evaluated independently on each RGB channel. All TV magnitudes are normalized by their maximum value and sorted in descending order. Thin curves correspond to individual decay profiles across images, channels, and directions. The blue solid curve denotes the mean decay, and the black solid curve denotes the median. Dashed curves indicate the 5%, 25%, 80%, and 95% percentile envelopes. The horizontal axis represents the normalized coefficient index (from largest to smallest), and the vertical axis shows the normalized TV magnitude on a logarithmic scale. The rapid and nearly identical decay observed in both spatial directions indicates that natural images possess effective sparsity in their spatial gradients: most variations are nonzero but contribute negligibly, while a small subset of dominant transitions captures the essential geometric structure.

Spectral Decay and Effective Sparsity in Textual Data

Unlike natural images, where sparsity typically manifests in fixed bases (e.g., wavelets), textual data exhibits sparsity within its latent semantic structures.

We analyze the spectral properties of term-document matrices constructed from the 20 Newsgroups [Mitchell \(1997\)](#) dataset. A key premise of our analysis, motivated by [Thibeault et al. \(2024\)](#), is that the textual information constituting a single coherent topic is inherently low-rank. To verify this, rather than analyzing global corpus statistics, we partition the documents into specific semantic categories (e.g., “sci.crypt”, “rec.sport.hockey”) and process them independently.

For each category, we construct a term-document matrix $\mathbf{x} \in \mathbb{R}^{n \times d}$ using TF-IDF features (including bigrams) without row-wise ℓ_2 normalization, thereby preserving magnitude information. We then perform the singular value decomposition (SVD). The functional information content is quantified by the normalized energy of the singular values:

$$\lambda_k = \frac{\sigma_k^2}{\sigma_1^2},$$

which corresponds to the eigenvalues of the empirical covariance matrix.

Figure 3 illustrates the aggregated decay profiles across all categories. The horizontal axis represents the normalized rank index, and the vertical axis shows the normalized spectral energy on a logarithmic scale. The results demonstrate that the singular values exhibit effective sparsity: the spectrum follows a sharp, heavy-tailed decay characteristic of power-law distributions.

Although the ambient dimension of the vocabulary is extremely high ($d \approx 50,000$), the effective rank of the system remains low. This rapid drop in eigenvalues indicates that the majority of the semantic variance within a single topic is captured by a very small number of latent factors, while the long tail of non-zero singular values corresponds to noise or idiosyncratic word usage with minimal predictive power. This empirical evidence confirms that effective sparsity fundamentally governs the complexity of high-dimensional linguistic systems.

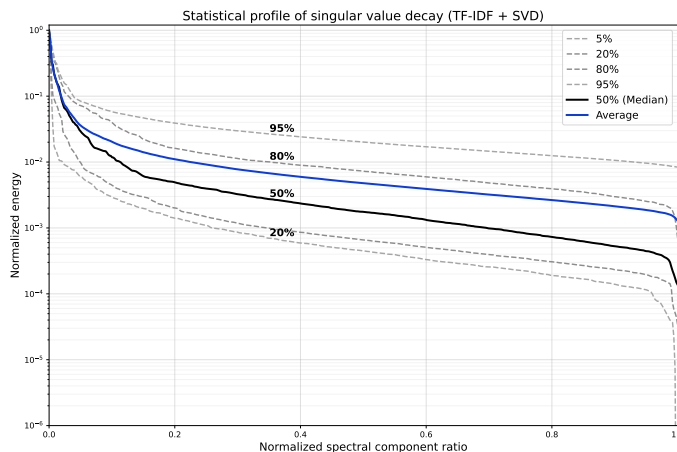


Figure 3: Effective sparsity in textual data (Spectral Decay). Aggregated spectral energy profiles of term-document matrices from the 20 Newsgroups dataset. For each text category, singular values σ_k were computed using TF-IDF vectorization and SVD; the curves plot the normalized energy $\sigma_k^2/\sigma_{\max}^2$. The blue solid line represents the mean decay across all categories, the black line represents the median, and the dashed lines indicate the 5%, 25%, 80%, and 95% percentile envelopes. The steep initial descent demonstrates that textual information within a single topic is low-rank, as meaningful semantic content is concentrated in a low-dimensional subspace (effective sparsity).

3 Effective Number of Nonzeros

3.1 Effective Nonzeros Metric

Sparse signal recovery aims to identify the most parsimonious solution of an underdetermined linear system (1.1). Classical sparsity-promoting approaches, such as Basis Pursuit or LASSO, seek solutions with minimal ℓ_1 or ℓ_0 norms. However, as discussed in the Section 1, these notions become fragile in practical regimes where signals are contaminated by small-amplitude perturbations. In such scenarios, the exact count of nonzero entries fails to capture the true information-theoretic complexity of the signal.

To address this, we formalize the distinction between exact nonzeros and effective nonzeros. For a vector $\mathbf{x} \in \mathbb{R}^n$, we define the normalized magnitude distribution $\boldsymbol{\pi}(\mathbf{x})$ with entries:

$$\pi_i(\mathbf{x}) = \frac{|x_i|}{\|\mathbf{x}\|_1}, \quad i = 1, \dots, n. \quad (3.1)$$

The associated Shannon entropy (measured in bits) is given by

$$\mathcal{H}(\mathbf{x}) = - \sum_{i=1}^n \pi_i(\mathbf{x}) \log_2 \pi_i(\mathbf{x}),$$

where we adopt the standard convention $0 \log_2 0 = 0$. We then define the ENZ as:

$$\text{ENZ}(\mathbf{x}) := 2^{\mathcal{H}(\mathbf{x})}. \quad (3.2)$$

The ENZ provides a continuous, magnitude-aware measure of sparsity that generalizes the discrete ℓ_0 norm. Unlike cardinality-based metrics, it depends on the normalized magnitude distribution $\boldsymbol{\pi}(\mathbf{x})$ and is therefore sensitive to how the ℓ_1 mass of \mathbf{x} is distributed across coordinates. If the entries of \mathbf{x} are exactly k -sparse and have equal magnitude on their support, then $\mathcal{H}(\mathbf{x}) = \log_2 k$ and thus $\text{ENZ}(\mathbf{x}) = k$, recovering $\|\mathbf{x}\|_0$. More generally, when the ℓ_1 mass of \mathbf{x} is overwhelmingly concentrated on a subset $S \subset \{1, \dots, n\}$ with $|S| = k$, the entropy $\mathcal{H}(\mathbf{x})$ remains close to $\log_2 k$, so that $\text{ENZ}(\mathbf{x})$ is close to k even if many additional coordinates are nonzero but have negligible amplitude. In this way, $\text{ENZ}(\mathbf{x})$ reflects the signal’s effective dimensionality while remaining robust to arbitrarily small perturbations that can dramatically change $\|\mathbf{x}\|_0$, a property that is crucial for stable recovery in the presence of modeling errors [Jaynes \(1957\)](#); [Cover \(1999\)](#); [Hurley and Rickard \(2009\)](#).

The advantage of the proposed metric can be further understood by examining the geometry of the ENZ ball. In sparse optimization, the geometry of a regularizer’s level sets determines the nature of the “prior” it imposes on the solution.

As illustrated in [Figure 4](#), the unit balls induced by ℓ_p quasi-norms ($0 < p \leq 1$) are bounded neighborhoods of the origin in \mathbb{R}^3 . While their cusp-like structure at the axes promotes sparsity, they share a fundamental limitation: their boundaries are closed and bounded. This implies that ℓ_p -type regularizers impose an increasing cost as coordinate magnitudes grow, inevitably leading to a magnitude shrinkage bias where significant signal components are suppressed along with the noise.

In contrast, the ENZ ball (the level set induced by the effective number of nonzeros) exhibits a qualitatively superior geometry. Since the ENZ is based on the normalized distribution of energy rather than absolute magnitudes, its level set manifests as an unbounded,

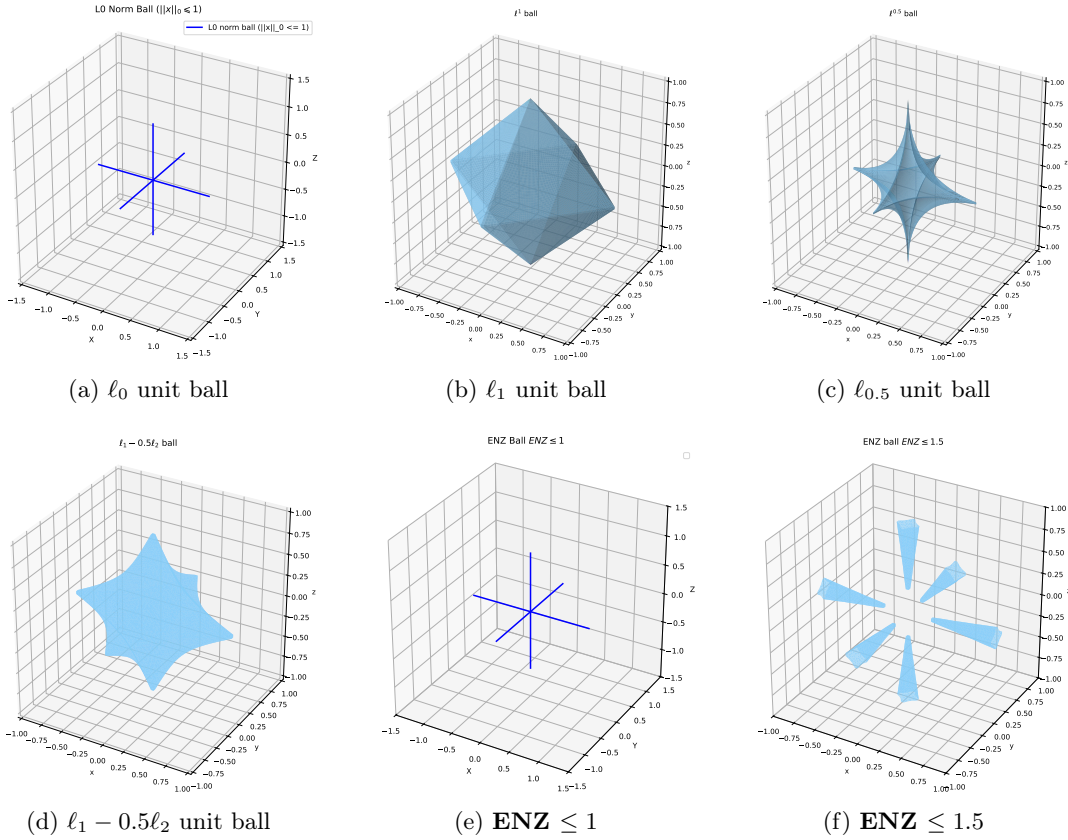


Figure 4: Visualization of level sets in \mathbb{R}^3 . The **ENZ ball** provides an unbounded, magnitude-aware geometry that directly generalizes the ℓ_0 norm while avoiding the shrinkage bias inherent in bounded ℓ_p balls.

star-shaped surface that asymptotically wraps around the coordinate axes. This geometry reveals two critical insights:

- **Decoupling Support from Magnitude:** Unlike the ℓ_p balls, the ENZ ball extends infinitely along the axes. This confirms that once a component is identified as part of the “effective support,” its magnitude can be recovered without the bias typical of shrinkage-based penalties.
- **Information-Theoretic Stability:** The ENZ ball excludes a neighborhood around the origin (the dense region) while providing a smooth transition for small-amplitude perturbations. This makes it a continuous and robust proxy for the discrete ℓ_0 “cross” (Figure 4a).

From this perspective, the ENZ ball bridges the gap between the combinatorial ideal of the ℓ_0 norm and the practical requirement for numerical stability. By using the ENZ as a metric, we recover the true sparsity structure while maintaining robustness to the “long tail” of negligible components.

3.2 ENZ Minimization and the Entropy Model

An ideal sparse recovery formulation based on effective nonzeros is given by:

$$\min_{\mathbf{x} \in \mathbb{R}^n} \text{ENZ}(\mathbf{x}) \quad \text{s.t.} \quad \|\mathbf{A}\mathbf{x} - \mathbf{b}\|_2^2 \leq \varepsilon. \quad (3.3)$$

In this constrained formulation, the parameter $\varepsilon > 0$ denotes a prescribed error tolerance. Theoretically, this value corresponds to the power of the additive noise. However, in practical scenarios where the exact noise level is often unknown, ε serves as a tunable hyperparameter representing an estimated upper bound on the residual energy.

However, the ENZ is a highly nonconvex function, which is difficult to optimize directly. Since the ENZ is a strictly monotonic transformation of the Shannon entropy, the minimization of $\text{ENZ}(\mathbf{x})$ is equivalent to minimizing $\mathcal{H}(\mathbf{x})$. This leads to the entropy-regularized sparse recovery model:

$$\min_{\mathbf{x} \in \mathbb{R}^n} \frac{1}{2} \|\mathbf{A}\mathbf{x} - \mathbf{b}\|_2^2 + \lambda \mathcal{H}(\mathbf{x}), \quad (3.4)$$

where $\lambda > 0$ is a regularization parameter.

3.3 Computational Motivation for Unnormalized Entropy

While $\mathcal{H}(\mathbf{x})$ directly characterizes the ENZ, its dependence on the ℓ_1 -normalization introduces analytical and computational hurdles that hinder stable and efficient optimization. Specifically, the normalization term $\|\mathbf{x}\|_1$ couples all coordinates of \mathbf{x} , which prevents the objective function from being separable and complicates the derivation of efficient proximal operators. To obtain a more stable and efficient optimization procedure, we introduce an *unnormalized entropy* surrogate. This surrogate decouples the coordinates and admits simple coordinate-wise updates that scale to large problems [Alabi et al. \(2023\)](#); [Abernethy and Rakhlin \(2009\)](#), while preserving the scale-invariance properties required for effective sparsity and yielding a smoother optimization landscape.

Assume the signal is bounded such that $|x_i| \leq C$ for some constant C . We define the scaled variables $z_i = |x_i|/C \in [0, 1]$ and the unnormalized entropy $\mathcal{H}_u(\mathbf{x})$ of \mathbf{x} as:

$$\mathcal{H}_u(\mathbf{x}) := - \sum_{i=1}^n \frac{|x_i|}{C} \log_2 \frac{|x_i|}{C} + \frac{\|\mathbf{x}\|_1}{C} = \frac{1}{C} \left(- \sum_{i=1}^n |x_i| \log_2 |x_i| + (1 + \log_2 C) \|\mathbf{x}\|_1 \right). \quad (3.5)$$

The normalized and unnormalized entropies are closely related:

$$\mathcal{H}_u(\mathbf{x}) = \frac{\|\mathbf{x}\|_1}{C} \left(\mathcal{H}(\mathbf{x}) + 1 + \log_2 \frac{C}{\|\mathbf{x}\|_1} \right).$$

In particular, when $C = \|\mathbf{x}\|_1$, we have

$$\mathcal{H}_u(\mathbf{x}) = \mathcal{H}(\mathbf{x}) + 1.$$

Therefore, $\mathcal{H}_u(\mathbf{x})$ serves as a convenient surrogate for $\mathcal{H}(\mathbf{x})$ in problems (3.3) and (3.4), while retaining the essential ENZ-minimization property. The function $h(z) = -z \log_2 z + z$ is smooth and strictly concave on \mathbb{R}_{++} , and \mathcal{H}_u inherits these properties. Crucially, \mathcal{H}_u is positively homogeneous of degree one, i.e., $\mathcal{H}_u(c\mathbf{x}) = c\mathcal{H}_u(\mathbf{x})$ for all $c > 0$.

4 Stability of Effective Sparsity under Restricted Isometry

In this section, we provide a rigorous stability analysis of signals characterized by their effective sparsity rather than their support. Traditional recovery guarantees in compressed sensing are often predicated on the assumption of exact k -sparsity, a condition that is frequently violated in practical applications due to numerical noise and modeling inaccuracies. We establish that if a sensing matrix A satisfies the Restricted Isometry Property (RIP), the recovery of the “effective nonzeros” remains stable, with error bounds gracefully determined by the energy of the negligible signal tail.

4.1 Problem Setup and Notation

Consider a sensing matrix $A \in \mathbb{R}^{m \times n}$ and two signals $\mathbf{x}, \mathbf{y} \in \mathbb{R}^n$ that satisfy the linear constraint $A\mathbf{x} = A\mathbf{y}$. We assume \mathbf{x} and \mathbf{y} are effectively k -sparse. To facilitate the analysis, we define the following sets and vectors:

- $S_x :=$ indices of the k largest (in magnitude) entries of \mathbf{x} , with S_x^c as its complement.
- $S_y :=$ indices of the k largest (in magnitude) entries of \mathbf{y} , with S_y^c as its complement.
- $T := S_x \cup S_y$ represents the union of the dominant supports, satisfying $|T| \leq 2k$ with T^c as its complement.

The difference vector is denoted by $\mathbf{h} := \mathbf{y} - \mathbf{x} \in \mathbb{R}^n$. For any index set $I \subset \{1, \dots, n\}$, we define \mathbf{h}_I as the sub-vector consisting of components indexed by I and zeros elsewhere. This allows the decomposition:

$$A\mathbf{h} = A\mathbf{h}_T + A\mathbf{h}_{T^c}.$$

4.2 Restricted Isometry Property (RIP)

The stability of recovery hinges on the Restricted Isometry Property (RIP) of order $2k$. Specifically, we assume A satisfies:

$$(1 - \delta_{2k})\|\mathbf{u}\|_2^2 \leq \|A\mathbf{u}\|_2^2 \leq (1 + \delta_{2k})\|\mathbf{u}\|_2^2, \quad \forall 2k\text{-sparse } \mathbf{u}. \quad (4.1)$$

where $\delta_{2k} \in (0, 1)$ denotes the (smallest) restricted isometry constant of order $2k$ associated with A , i.e., the smallest value such that (4.1) holds for all $2k$ -sparse vectors.

The following proposition summarizes essential properties derived from the $2k$ -RIP. The first inequality is a direct consequence of the *restricted eigenvalue (RE) condition* [Bickel et al. \(2009\)](#) or the *sparse eigenvalue condition* [Meinshausen and Yu \(2009\)](#); [Bunea et al. \(2007\)](#), which are used to establish oracle inequalities and recovery guarantees for the Lasso and related estimators. Part (ii) is from [Candes and Tao \(2005\)](#) and ([Candès, 2008](#), Lemma 2.1).

Proposition 1 *Suppose $A \in \mathbb{R}^{m \times n}$ satisfies the $2k$ -RIP (4.1).*

- (i) *For every index set T with $|T| \leq 2k$, the restricted matrix A_T satisfies the lower singular value bound:*

$$\sigma_{\min}(A_T) \geq \sqrt{1 - \delta_{2k}} > 0. \quad (4.2)$$

(ii) Let $\mathbf{u}, \mathbf{v} \in \mathbb{R}^n$ have disjoint supports such that $|\text{supp}(\mathbf{u})| + |\text{supp}(\mathbf{v})| \leq 2k$. Then:

$$|\langle A\mathbf{u}, A\mathbf{v} \rangle| \leq \delta_{2k} \|\mathbf{u}\|_2 \|\mathbf{v}\|_2.$$

4.3 Stability Analysis under Noisy Measurements

To formalize effective sparsity in the noisy setting, we model each signal by its top- k dominant entries plus a small tail. In particular, we quantify the tail energy outside the top- k index sets S_x and S_y by the following conditions:

$$\|\mathbf{x}_{S_x^c}\|_2 \leq \varepsilon_x, \quad \|\mathbf{y}_{S_y^c}\|_2 \leq \varepsilon_y. \quad (4.3)$$

We next consider the noisy observation model $A\mathbf{x} + \boldsymbol{\eta} = A\mathbf{y} + \boldsymbol{\eta}'$, where $\boldsymbol{\eta}, \boldsymbol{\eta}' \in \mathbb{R}^m$ represent measurement noise or modeling errors. Defining the effective noise as $\mathbf{e} := \boldsymbol{\eta} - \boldsymbol{\eta}'$, the discrepancy vector satisfies $A\mathbf{h} = \mathbf{e}$.

Our goal is to show that if A is sufficiently well-conditioned on all $2k$ -column submatrices—formalized via the RIP or a lower singular value bound—then the dominant coordinates of \mathbf{x} and \mathbf{y} must remain close. This extends the classical uniqueness results of sparse recovery to the regime of approximately sparse vectors [Blanchard et al. \(2011\)](#); [Candès et al. \(2006\)](#); [Donoho \(2006\)](#); [Candès and Wakin \(2008\)](#).

Theorem 2 formalizes this intuition. It demonstrates that as long as A does not collapse any $2k$ -sparse vector, any two signals with k effective nonzeros will possess similar values on their primary supports. Crucially, this stability is maintained even if the literal ℓ_0 norm of the signals significantly exceeds k . The resulting error bound is explicitly controlled by the aggregate tail energy $\varepsilon_x + \varepsilon_y$ and the restricted condition number of A . This confirms a key trade-off: while effective nonzeros provide robustness to small perturbations, they necessitate a measurement matrix that is stable across the entire effective support union.

Theorem 2 (Stability of the Effective Nonzeros under Noise) *Let $A \in \mathbb{R}^{m \times n}$ satisfy the $2k$ -RIP (4.1) with constant $\delta_{2k} \in (0, 1)$. Let $\mathbf{x}, \mathbf{y} \in \mathbb{R}^n$ be two signals, and define:*

- $S_x, S_y \subset \{1, \dots, n\}$: the index sets of the k largest-magnitude entries of \mathbf{x} and \mathbf{y} , respectively;
- $T := S_x \cup S_y$ (so $|T| \leq 2k$) and $\mathbf{h} := \mathbf{y} - \mathbf{x}$.

Assume the tail conditions

$$\|\mathbf{x}_{S_x^c}\|_2 \leq \varepsilon_x, \quad \|\mathbf{y}_{S_y^c}\|_2 \leq \varepsilon_y,$$

and suppose there exists $\mathbf{e} \in \mathbb{R}^m$ such that $A\mathbf{h} = \mathbf{e}$ (i.e., $A\mathbf{x}$ and $A\mathbf{y}$ differ by \mathbf{e}). Under the assumptions above, the difference between \mathbf{x} and \mathbf{y} on the union of their top- k supports satisfies

$$\|\mathbf{h}_T\|_2 \leq \frac{\sqrt{2(n-2k)} \delta_{2k}}{(1-\delta_{2k})\sqrt{k}} (\varepsilon_x + \varepsilon_y) + \frac{\sqrt{1+\delta_{2k}}}{(1-\delta_{2k})} \|\mathbf{e}\|_2. \quad (4.4)$$

Consequently, the effective nonzeros of \mathbf{x} and \mathbf{y} satisfy

$$\|\mathbf{x}_{S_x} - \mathbf{y}_{S_y}\|_2 \leq \left(\frac{\sqrt{2(n-2k)} \delta_{2k}}{(1-\delta_{2k})\sqrt{k}} + 1 \right) (\varepsilon_x + \varepsilon_y) + \frac{\sqrt{1+\delta_{2k}}}{(1-\delta_{2k})} \|\mathbf{e}\|_2. \quad (4.5)$$

Proof Starting from $A\mathbf{h} = A(\mathbf{y} - \mathbf{x}) = \mathbf{e}$ and $A\mathbf{h}_T = -A\mathbf{h}_{T^c} + \mathbf{e}$. We further decompose \mathbf{h}_T as

$$\mathbf{h}_T = \mathbf{u} + \mathbf{v}, \quad \mathbf{u} := \mathbf{h}_{S_x}, \quad \mathbf{v} := \mathbf{h}_{S_y \setminus S_x}.$$

Observe that \mathbf{u} and \mathbf{v} are at most k -sparse and have disjoint supports. It follows that $\|\mathbf{h}_T\|_2^2 = \|\mathbf{u}\|_2^2 + \|\mathbf{v}\|_2^2$. Next, partition the tail \mathbf{h}_{T^c} into blocks B_1, B_2, \dots of size at most k , sorted in decreasing order of magnitude. By standard sorted-tail inequalities, for any $j \geq 2$,

$$\|\mathbf{h}_{B_j}\|_2 \leq \frac{\|\mathbf{h}_{B_{j-1}}\|_1}{\sqrt{k}}.$$

Summing up both sides yields

$$\sum_{j \geq 1} \|\mathbf{h}_{B_j}\|_2 \leq \frac{\|\mathbf{h}_{T^c}\|_1}{\sqrt{k}}. \quad (4.6)$$

Fix any block $B_j \subseteq T^c$ with $|B_j| \leq k$. Since each of $\text{supp}(\mathbf{u})$ and $\text{supp}(\mathbf{v})$ has size $\leq k$ and is disjoint from B_j , the standard RIP-based cross-term bound Proposition 1(ii) applies to the pairs $(\mathbf{u}, \mathbf{h}_{B_j})$ and $(\mathbf{v}, \mathbf{h}_{B_j})$:

$$|\langle A\mathbf{u}, A\mathbf{h}_{B_j} \rangle| \leq \delta_{2k} \|\mathbf{u}\|_2 \|\mathbf{h}_{B_j}\|_2, \quad |\langle A\mathbf{v}, A\mathbf{h}_{B_j} \rangle| \leq \delta_{2k} \|\mathbf{v}\|_2 \|\mathbf{h}_{B_j}\|_2.$$

Summing yields

$$|\langle A\mathbf{h}_T, A\mathbf{h}_{B_j} \rangle| = |\langle A(\mathbf{u} + \mathbf{v}), A\mathbf{h}_{B_j} \rangle| \leq \delta_{2k} (\|\mathbf{u}\|_2 + \|\mathbf{v}\|_2) \|\mathbf{h}_{B_j}\|_2.$$

Using $\|\mathbf{u}\|_2 + \|\mathbf{v}\|_2 \leq \sqrt{2} \sqrt{\|\mathbf{u}\|_2^2 + \|\mathbf{v}\|_2^2} = \sqrt{2} \|\mathbf{h}_T\|_2$, we obtain the bound

$$|\langle A\mathbf{h}_T, A\mathbf{h}_{B_j} \rangle| \leq \sqrt{2} \delta_{2k} \|\mathbf{h}_T\|_2 \|\mathbf{h}_{B_j}\|_2. \quad (4.7)$$

On the other hand, from $A\mathbf{h} = \mathbf{e}$ (i.e. $A\mathbf{h}_T + A\mathbf{h}_{T^c} = \mathbf{e}$), we have

$$A\mathbf{h}_T = -\sum_{j \geq 1} A\mathbf{h}_{B_j} + \mathbf{e}.$$

Take the squared norm and apply the RIP lower bound on \mathbf{h}_T (note $|\text{supp}(\mathbf{h}_T)| \leq 2k$):

$$(1 - \delta_{2k}) \|\mathbf{h}_T\|_2^2 \leq \|A\mathbf{h}_T\|_2^2 = \left\langle A\mathbf{h}_T, -\sum_{j \geq 1} A\mathbf{h}_{B_j} + \mathbf{e} \right\rangle = -\sum_{j \geq 1} \langle A\mathbf{h}_T, A\mathbf{h}_{B_j} \rangle + \langle A\mathbf{h}_T, \mathbf{e} \rangle. \quad (4.8)$$

It follows from (4.7) and the triangle inequality that

$$(1 - \delta_{2k}) \|\mathbf{h}_T\|_2^2 \leq \sum_{j \geq 1} |\langle A\mathbf{h}_T, A\mathbf{h}_{B_j} \rangle| + |\langle A\mathbf{h}_T, \mathbf{e} \rangle| \leq \sqrt{2} \delta_{2k} \|\mathbf{h}_T\|_2 \sum_{j \geq 1} \|\mathbf{h}_{B_j}\|_2 + |\langle A\mathbf{h}_T, \mathbf{e} \rangle|.$$

Dividing both sides by $(1 - \delta_{2k}) \|\mathbf{h}_T\|_2$ (the case $\mathbf{h}_T = 0$ is trivial), we obtain from (4.6)

$$\|\mathbf{h}_T\|_2^2 \leq \frac{\sqrt{2} \delta_{2k}}{1 - \delta_{2k}} \sum_{j \geq 1} \|\mathbf{h}_{B_j}\|_2 + \frac{|\langle A\mathbf{h}_T, \mathbf{e} \rangle|}{(1 - \delta_{2k}) \|\mathbf{h}_T\|_2} \leq \frac{\sqrt{2} \delta_{2k}}{1 - \delta_{2k}} \frac{\|\mathbf{h}_{T^c}\|_1}{\sqrt{k}} + \frac{|\langle A\mathbf{h}_T, \mathbf{e} \rangle|}{(1 - \delta_{2k}) \|\mathbf{h}_T\|_2}. \quad (4.9)$$

By Cauchy-Schwarz inequality and the lower RIP bound, we have

$$\begin{aligned}\|\mathbf{h}_{T^c}\|_1 &\leq \|\mathbf{x}_{T^c}\|_1 + \|\mathbf{y}_{T^c}\|_1 \leq \sqrt{|T^c|}(\|\mathbf{x}_{T^c}\|_2 + \|\mathbf{y}_{T^c}\|_2) \leq (n - |T| \leq n - 2k)(\varepsilon_x + \varepsilon_y) \\ |\langle A\mathbf{h}_T, \mathbf{e} \rangle| &\leq \|A\mathbf{h}_T\|_2 \|\mathbf{e}\|_2 \leq \sqrt{1 + \delta_{2k}} \|\mathbf{h}_T\|_2 \|\mathbf{e}\|_2.\end{aligned}$$

Plugging in (4.9), we obtain (4.4).

Finally, to compare the effective k nonzeros, we write:

$$\mathbf{x}_{S_x} - \mathbf{y}_{S_y} = (\mathbf{x} - \mathbf{y})_T + \mathbf{x}_{S_y \setminus S_x} - \mathbf{y}_{S_x \setminus S_y},$$

Note that $S_y \setminus S_x \subset S_x^c$ and $S_x \setminus S_y \subset S_y^c$. Therefore, the additional terms are bounded by the tail norms ε_x and ε_y respectively. Applying the triangle inequality and (4.4) completes the proof. \blacksquare

Remark: Theoretical Significance of Effective Nonzeros

Theorem 2 provides a formal justification for the use of effective nonzeros in sparse recovery. Classical RIP requirements typically scale with the apparent sparsity. Attempting to protect every infinitesimal nonzero component forces δ_t conditions for $t \gg 2k$, which are harder to satisfy and require significantly more measurements. Theorem 2 demonstrates that as long as the matrix is well-conditioned on the $2k$ -dominant subspace, stable recovery is guaranteed despite the presence of pervasive “speckle” noise or numerical artifacts. This ensures that theoretical conditions and sampling resources are dedicated solely to the aspects of the solution that truly matter for interpretation and computation.

5 Decomposition of the Effective Number of Nonzeros

In this section, we derive an exact decomposition for the ENZ, revealing it as an information-theoretic “softening” of the ℓ_0 norm. This structural result demonstrates that ENZ does not merely approximate ℓ_0 ; rather, it discounts the contribution of each nonzero component based on its relative energy concentration.

We begin with the Shannon entropy formulation, which offers the most transparent geometric interpretation.

Theorem 3 (Decomposition of Effective Nonzeros) *Let $\mathbf{x} \in \mathbb{R}^n \setminus \{0\}$, and let $\boldsymbol{\pi}$ be the normalized magnitude distribution where $\pi_i = |x_i|/\|\mathbf{x}\|_1$. Let $S = \text{Supp}(\mathbf{x})$ and denote \mathbf{u} as the uniform distribution over S , i.e., $u_i = 1/|S|$ for $i \in S$. The normalized Shannon entropy $\mathcal{H}(\mathbf{x})$ admits the following decomposition:*

$$\mathcal{H}(\mathbf{x}) = \log_2 \|\mathbf{x}\|_0 - D_{\text{KL}}(\boldsymbol{\pi} \|\mathbf{u}). \quad (5.1)$$

Consequently, the effective number of nonzeros satisfies:

$$\text{ENZ}(\mathbf{x}) := 2^{\mathcal{H}(\mathbf{x})} = \|\mathbf{x}\|_0 \cdot \exp_2(-D_{\text{KL}}(\boldsymbol{\pi} \|\mathbf{u})), \quad (5.2)$$

where $D_{\text{KL}}(\boldsymbol{\pi} \|\mathbf{u}) \geq 0$ is the Kullback-Leibler divergence. Equality holds if and only if $|x_i|$ is constant for all $i \in S$.

coordinate-wise, entropy regularization acts globally on the normalized amplitude distribution. Consequently, it simultaneously penalizes the expansion of the support and the proliferation of insignificant, noise-like coefficients.

Remark 5 (Hartley Entropy and the ℓ_0 Limit) *The ℓ_0 norm can be elegantly situated within this information-theoretic framework as a limiting case. In the literature, the Hartley entropy (or Rényi entropy of order zero) of a discrete distribution is defined as the logarithm of the support size [Hartley \(1928\)](#). For any $\mathbf{x} \in \mathbb{R}^n$, we have:*

$$\mathcal{H}_h(\mathbf{x}) = \log_2 \|\mathbf{x}\|_0, \quad \text{and} \quad \text{ENZ}_0(\mathbf{x}) = 2^{\mathcal{H}_h(\mathbf{x})} = \|\mathbf{x}\|_0.$$

This connection further confirms that our framework provides a unified view of sparsity. The classical ℓ_0 norm represents a maximum-entropy scenario where all components are assumed equally significant, while ENZ refines this measure by accounting for the true informational concentration of the signal.

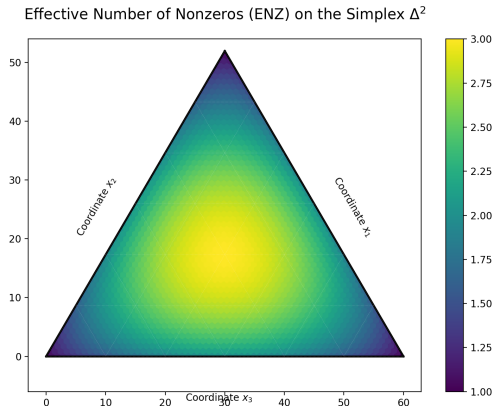


Figure 6: The landscape of the ENZ on the 2-simplex Δ^2 . The vertices represent 1-sparse signals where $D_{\text{KL}}(\boldsymbol{\pi} \|\mathbf{u})$ is maximized relative to a 3-element support, leading to $\text{ENZ} = 1$. The barycenter represents the uniform distribution where $D_{\text{KL}} = 0$ and $\text{ENZ} = 3$. This heatmap illustrates how the ENZ smoothly “softens” the ℓ_0 norm, penalizing the effective dimensionality as the signal moves away from the uniform support toward the manifold of lower-cardinality signals.

6 A Unified Family of Sparsity Measures: The Rényi ENZ

While the Shannon entropy provides a natural proxy for effective sparsity, it represents only a single point in the broader spectrum of information-theoretic functions. In this section, we generalize our framework to the Rényi entropy family, developing a unified class of sparsity measures that encompasses several well-known penalties in compressed sensing as special cases.

Rényi entropy introduces a tunable parameter α , which allows for a controlled emphasis on different regions of the signal’s magnitude distribution. This flexibility is particularly

advantageous for quantifying sparsity in high-dimensional settings where the sensitivity to the “tail” versus the “peak” of the distribution is critical.

6.1 The Rényi Effective Number of Nonzeros (Rényi ENZ)

The Rényi entropy of order α ($\alpha > 0, \alpha \neq 1$) is defined as:

$$\mathcal{R}_\alpha(\mathbf{x}) = \frac{1}{1-\alpha} \log_2 \left(\sum_{i=1}^n \pi_i^\alpha \right). \quad (6.1)$$

By varying α , one can interpolate between different notions of concentration. Specifically, as α increases, the entropy becomes increasingly sensitive to the dominant components, whereas smaller values of α provide a more democratic assessment of the signal’s support.

Analogous to the Shannon ENZ, we define the **Rényi Effective Number of Nonzeros (Rényi ENZ)** as:

$$\text{ENZ}_\alpha^R(\mathbf{x}) := 2^{\mathcal{R}_\alpha(\mathbf{x})} = \left(\sum_{i=1}^n \pi_i^\alpha \right)^{\frac{1}{1-\alpha}}. \quad (6.2)$$

This quantity provides a parameterized family of sparsity measures that inhabit the space between literal support cardinality and energy concentration.

6.2 General Decomposition and the Hierarchy of Sparsity

The relationship between Rényi ENZ and the ℓ_0 norm is characterized by the following generalization of the decomposition theorem.

Theorem 6 (Generalized Rényi Decomposition) *Let $\mathbf{x} \in \mathbb{R}^n \setminus \{0\}$ and let \mathbf{u} be the uniform distribution over $S = \text{supp}(\mathbf{x})$. For any $\alpha > 0, \alpha \neq 1$, the Rényi entropy admits the decomposition:*

$$\mathcal{R}_\alpha(\mathbf{x}) = \log_2 \|\mathbf{x}\|_0 - D_\alpha(\boldsymbol{\pi} \|\mathbf{u}), \quad (6.3)$$

where $D_\alpha(\boldsymbol{\pi} \|\mathbf{u}) = \frac{1}{\alpha-1} \log_2(\sum_{i \in S} \pi_i^\alpha u_i^{1-\alpha})$ is the Rényi divergence of order α . Consequently, the Rényi ENZ satisfies the multiplicative relation:

$$\text{ENZ}_\alpha^R(\mathbf{x}) = \|\mathbf{x}\|_0 \cdot 2^{-D_\alpha(\boldsymbol{\pi} \|\mathbf{u})} \leq \|\mathbf{x}\|_0. \quad (6.4)$$

6.3 Recovering Classical Penalties: The Sparsity Hierarchy

The Rényi ENZ family is remarkably expressive, recovering several “industry-standard” sparsity measures as α takes specific values:

- **The Shannon Limit** ($\alpha \rightarrow 1$): Recovers the Shannon ENZ, $\text{ENZ}(\mathbf{x}) = 2^{\mathcal{H}(\mathbf{x})}$, providing the most balanced information-theoretic measure.
- **The ℓ_1/ℓ_2 Ratio** ($\alpha = 2$): The second-order ENZ (Collision ENZ) corresponds exactly to the square of the ℓ_1/ℓ_2 ratio:

$$\text{ENZ}_2^R(\mathbf{x}) = \frac{\|\mathbf{x}\|_1^2}{\|\mathbf{x}\|_2^2}.$$

This establishes a formal information-theoretic interpretation for the scale-invariant ℓ_1/ℓ_2 penalty widely used in sparse optimization.

- **The ℓ_1/ℓ_∞ Ratio ($\alpha \rightarrow \infty$):** In the limit of infinite order, the measure depends only on the peak magnitude, yielding $\text{ENZ}_\infty^R(\mathbf{x}) = \|\mathbf{x}\|_1/\|\mathbf{x}\|_\infty$.
- **The ℓ_0 Limit ($\alpha \rightarrow 0$):** As the order approaches zero, the measure becomes indifferent to magnitudes, recovering the discrete cardinality: $\lim_{\alpha \rightarrow 0} \text{ENZ}_\alpha^R(\mathbf{x}) = \|\mathbf{x}\|_0$.

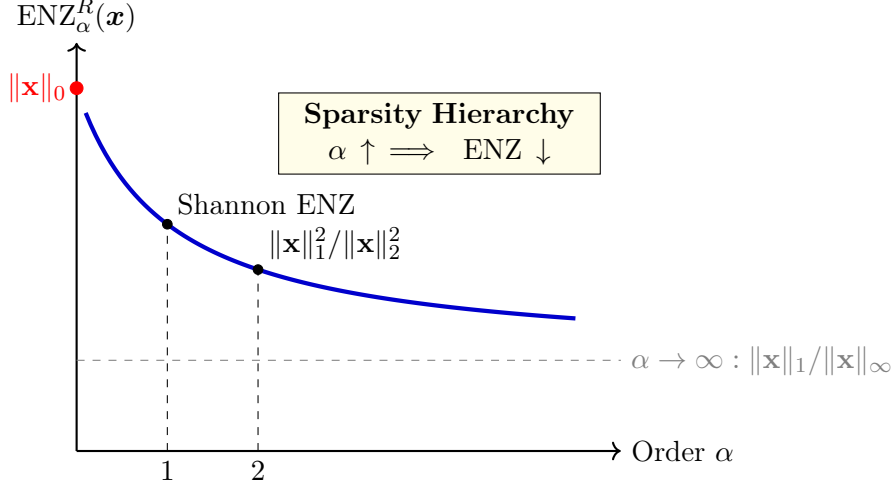


Figure 7: The Rényi ENZ spectrum as a function of order α . The measure provides a continuous interpolation between the combinatorial ℓ_0 norm ($\alpha \rightarrow 0$) and the scale-invariant ratio $\|\mathbf{x}\|_1/\|\mathbf{x}\|_\infty$ ($\alpha \rightarrow \infty$).

Crucially, the Rényi ENZ satisfies a monotonicity property with respect to α . For any signal \mathbf{x} , we have the following fundamental hierarchy of effective sparsity:

$$\|\mathbf{x}\|_0 \geq \text{ENZ}_{\text{Shannon}}(\mathbf{x}) \geq \frac{\|\mathbf{x}\|_1^2}{\|\mathbf{x}\|_2^2} \geq \frac{\|\mathbf{x}\|_1}{\|\mathbf{x}\|_\infty}. \quad (6.5)$$

The hierarchical structure of the Rényi ENZ is visually encapsulated in Figure 7. As the order α increases, the ENZ spectrum exhibits a strictly monotonic decreasing property, effectively “scanning” the signal from its combinatorial support toward its peak concentration. Specifically, for any signal \mathbf{x} , we observe the following fundamental sparsity hierarchy corresponding to the landmark points on the curve:

$$\|\mathbf{x}\|_0 \xrightarrow{\alpha \rightarrow 0} \text{ENZ}_{\text{Shannon}}(\mathbf{x}) \xrightarrow{\alpha=1} \frac{\|\mathbf{x}\|_1^2}{\|\mathbf{x}\|_2^2} \xrightarrow{\alpha=2} \dots \xrightarrow{\alpha \rightarrow \infty} \frac{\|\mathbf{x}\|_1}{\|\mathbf{x}\|_\infty}. \quad (6.6)$$

This spectrum provides a rigorous roadmap for sparse regularization as depicted in the figure:

- **High-sensitivity regime ($\alpha \rightarrow 0$):** The measure approaches the “ideal” but numerically brittle ℓ_0 norm (the red intercept in Figure 7).

- **Balanced regime** ($\alpha \in [1, 2]$): The Shannon ENZ and the ℓ_1/ℓ_2 ratio provide smooth, stable surrogates that are easier to optimize while still penalizing effective support.
- **Asymptotic regime** ($\alpha \rightarrow \infty$): The curve flattens toward its lower bound (the gray dashed horizontal asymptote), representing the most aggressive “peak-centric” sparsity measure.

By selecting a specific α , we can traverse this curve to navigate the trade-offs between exact support recovery and computational tractability.

While this normalized construction yields a clear hierarchy and interpretable limits, it also introduces a coupling across coordinates through the normalization $\pi_i = |x_i|/\|\mathbf{x}\|_1$. That global coupling obscures separability and complicates proximal optimization. To preserve the Rényi spectrum while recovering coordinate-wise structure, we now introduce an unnormalized variant that removes the normalization constraint.

6.4 Unnormalized Rényi Entropy and the Tsallis Connection

Following the motivation for the Shannon case, we observe that the standard Rényi entropy $\mathcal{R}_\alpha(\mathbf{x})$ suffers from two structural bottlenecks that hinder optimization. First, the global normalization $\pi_i = |x_i|/\|\mathbf{x}\|_1$ introduces a coupling across all coordinates, destroying separability. Second, the outer logarithm prevents the function from being expressed as a simple sum of coordinate-wise scalar functions. Both of these traits complicate the application of fast, proximal-splitting algorithms.

To construct an optimization-friendly surrogate, we take a two-step approach to preserve the spectral sensitivity of the Rényi family while recovering coordinate-wise structure.

From Rényi to Tsallis (Removing the Logarithm). Recall that Rényi entropy is a logarithmic transform of an α -power sum. In information theory, the non-logarithmic relaxation of Rényi entropy naturally yields the Tsallis entropy Tsallis (1988). For a probability distribution $\boldsymbol{\pi}$, the Tsallis entropy is defined as $S_\alpha(\boldsymbol{\pi}) = \frac{1}{\alpha-1}(1 - \sum_{i=1}^n \pi_i^\alpha)$. Since $\sum_{i=1}^n \pi_i = 1$, we can cleanly rewrite this centering as:

$$S_\alpha(\boldsymbol{\pi}) = \frac{1}{1-\alpha} \sum_{i=1}^n (\pi_i^\alpha - \pi_i). \quad (6.7)$$

Coordinate-wise Decoupling. To break the global coupling induced by π_i , we abandon the probability normalization $\sum \pi_i = 1$. Instead, we introduce a fixed, independent scaling constant $C > 0$ such that $C \geq \|\mathbf{x}\|_\infty$ (e.g., an upper bound on the signal’s peak magnitude or the dominant singular value $\|A\|_2$ in the matrix case). By replacing the coupled probability π_i with the decoupled fraction $\frac{|x_i|}{C} \in [0, 1]$, we preserve the bounded nature of the inputs while achieving strict separability.

Motivated by the Tsallis centering above, but properly scaled by C to match the magnitude of \mathbf{x} , we define the **unnormalized Rényi entropy** of order α ($\alpha > 0, \alpha \neq 1$) as:

$$\mathcal{R}_{u,\alpha}(\mathbf{x}; C) := \frac{C}{1-\alpha} \sum_{i=1}^n \left(\left(\frac{|x_i|}{C} \right)^\alpha - \frac{|x_i|}{C} \right) = \frac{1}{1-\alpha} (C^{1-\alpha} \|\mathbf{x}\|_\alpha^\alpha - \|\mathbf{x}\|_1). \quad (6.8)$$

The subtraction of the linear term $\frac{|x_i|}{C}$ is structurally critical; it acts as the precise analogue of the “−1” in standard Tsallis entropy, ensuring consistent behavior across different orders of α . This scaled formulation provides a unified, separable landscape for optimization, connecting several classical penalties through the continuous parameter α :

- **The Counting Limit** ($\alpha \rightarrow 0$): Since $(|x_i|/C)^\alpha \rightarrow \mathbf{1}_{\{x_i \neq 0\}}$, the function converges to:

$$\lim_{\alpha \rightarrow 0} \mathcal{R}_{u,\alpha}(\mathbf{x}; C) = C\|\mathbf{x}\|_0 - \|\mathbf{x}\|_1.$$

This objective is proportional to the literal support size (ℓ_0 -norm), regularized by a linear bias tied to the signal’s amplitude. It suggests that for small α , the function acts as a smoothed rank/support approximation, where C acts as a trade-off parameter between strict counting and magnitude suppression.

- **The Shannon Limit** ($\alpha \rightarrow 1$): Applying L’Hôpital’s rule with respect to α (with the convention $0 \ln 0 := 0$), the derivative of the numerator yields $C(|x_i|/C)^\alpha \ln(|x_i|/C)$, resulting perfectly in:

$$\lim_{\alpha \rightarrow 1} \mathcal{R}_{u,\alpha}(\mathbf{x}; C) = - \sum_{i=1}^n |x_i| \ln \left(\frac{|x_i|}{C} \right).$$

This matches the coordinate-wise unnormalized Shannon entropy discussed in Section 6, confirming that our Tsallis-inspired construction is a rigorous, consistent generalization.

- **The Energy-Sparsity Trade-off** ($\alpha = 2$): Setting $\alpha = 2$ yields a purely algebraic, highly interpretable function:

$$\mathcal{R}_{u,2}(\mathbf{x}; C) = \|\mathbf{x}\|_1 - \frac{1}{C}\|\mathbf{x}\|_2^2.$$

Minimizing this objective creates a powerful “push-pull” dynamic. It simultaneously imposes pressure to reduce the ℓ_1 -norm (promoting exact zeros) while maximizing the ℓ_2 -norm (preserving concentrated signal energy). In the matrix context, this corresponds to minimizing $\|A\|_* - \frac{1}{C}\|A\|_F^2$. This encourages the signal to condense its energy into the fewest possible components, effectively attempting to maximize the Frobenius norm relative to the nuclear norm proxy.

Ultimately, $\mathcal{R}_{u,\alpha}(\mathbf{x}; C)$ provides a separable continuous homotopy of sparsity-inducing regularizers. By tuning α , we can seamlessly interpolate between combinatorial counting ($\alpha \approx 0$), information-theoretic logarithmic compression ($\alpha \approx 1$), and quadratic energy concentration ($\alpha = 2$), without introducing the global coupling inherent to probability normalization.

7 Numerical Experiments

This section studies entropy-based regularization for sparse recovery and image denoising. All experiments use the unconstrained penalized formulation

$$\min_{\mathbf{x} \in \mathbb{R}^n} J(\mathbf{x}) := \frac{1}{2}\|A\mathbf{x} - \mathbf{b}\|_2^2 + \lambda H_u(\mathbf{x}). \quad (7.1)$$

where H_u denotes the proposed unnormalized entropy regularizer in (3.5) and $\lambda > 0$ is the regularization parameter.

7.1 Sparse Signal Recovery

We first evaluate the method on compressed sensing problems in the underdetermined regime ($m \ll n$). The measurement matrix $A \in \mathbb{R}^{m \times n}$ is generated from a correlated Gaussian ensemble. Each row is sampled independently from $\mathcal{N}(\mathbf{0}, \Sigma)$ with covariance

$$\Sigma_{ij} = (1 - r)\delta_{ij} + r, \quad r \in [0, 1].$$

Unless otherwise stated, we use $m = 64$, $n = 512$, and $r = 0.1$. The ground-truth signal $\mathbf{x}^* \in \mathbb{R}^n$ is generated as a k -sparse vector. The support is selected uniformly at random, and nonzero entries are sampled independently from $\mathcal{N}(0, 1)$. To study recovery under large amplitude variation, the nonzero coefficients are rescaled to achieve a prescribed dynamic range

$$C_r = \log_{10} \left(\frac{\max |\mathbf{x}^*|}{\min |\mathbf{x}^*|} \right).$$

Unless otherwise specified, $C_r = 3$. Measurements are generated according to

$$\mathbf{b} = A\mathbf{x}^* + \boldsymbol{\varepsilon}, \tag{7.2}$$

where $\boldsymbol{\varepsilon}$ is Gaussian noise with variance chosen such that

$$\|\boldsymbol{\varepsilon}\|_2 = \eta \|A\mathbf{x}^*\|_2,$$

with $\eta \in \{0.01, 0.02, 0.03\}$.

We compare the proposed unnormalized entropy regularization 3.5 (with $C = \|\mathbf{x}\|_2$) with three baselines: ℓ_0 , ℓ_1 , and the log-sum penalty. For each regularizer, we employ a standard solver commonly used for that model class: IHT for ℓ_0 , ISTA for the convex ℓ_1 problem, and IRL1 for the nonconvex log-sum penalty.

In our implementation we set $C = \|\mathbf{x}\|_2$, but we freeze C when computing the gradient within each outer iteration. Specifically, at outer iteration t we fix $C^{(t)} = \|\mathbf{x}^{(t)}\|_2$ and minimize the resulting smooth surrogate objective with respect to \mathbf{x} using L-BFGS, treating $C^{(t)}$ as a constant. After obtaining the updated iterate, we update the scale as $C^{(t+1)} = \|\mathbf{x}^{(t+1)}\|_2$ and repeat. This yields an iterative re-scaling (fixed-point) scheme while keeping the inner optimization smooth and well-conditioned.

For entropy regularization, we employ a smooth approximation by replacing $|x_i|$ with $\sqrt{x_i^2 + \epsilon}$, which leads (for fixed C) to

$$\frac{\partial \mathcal{H}_{u,\epsilon}}{\partial x_i} = -\frac{1}{C} \ln \left(\frac{\sqrt{x_i^2 + \epsilon}}{C} \right) \frac{x_i}{\sqrt{x_i^2 + \epsilon}}.$$

We minimize the resulting smooth objective using L-BFGS together with an ϵ -continuation schedule, starting from a relatively large ϵ and gradually decreasing it to better approximate

the original nonsmooth entropy penalty. For all methods, λ is chosen by logarithmic grid search over $[10^{-3}, 10^5]$.

The value minimizing the relative reconstruction error

$$\text{Err}(\hat{\mathbf{x}}) = \frac{\|\hat{\mathbf{x}} - \mathbf{x}^*\|_2}{\|\mathbf{x}^*\|_2}$$

is reported. For N independent Monte Carlo trials, we declare trial t successful if the relative reconstruction error satisfies

$$\text{Err}(\hat{\mathbf{x}}) \leq \tau,$$

where $\tau = 0.05$. The empirical success rate is then computed as

$$\frac{1}{N} \sum_{t=1}^N \mathbb{I}_t,$$

where \mathbb{I}_t is the indicator of success for trial t , defined by

$$\mathbb{I}_t = \begin{cases} 1, & \text{if } \text{Err}(\hat{\mathbf{x}}) \leq \tau, \\ 0, & \text{otherwise,} \end{cases} \quad t = 1, \dots, N.$$

Figure 8 summarizes the empirical success rates. In this setting, entropy regularization yields consistently higher success rates than ℓ_1 and log-sum across the tested noise levels, indicating improved robustness to measurement noise for signals with large dynamic range.

7.2 Image Denoising

PROBLEM FORMULATION BASED ON DISCRETE GRADIENTS

We formulate the image denoising problem using a variational approach based on discrete image differences. Let $\mathbf{y} \in \mathbb{R}^N$ denote the vectorized observed noisy image and $\mathbf{x} \in \mathbb{R}^N$ be the latent clean image, where $N = H \times W$. The discrete gradient operator $\mathbf{D} \in \mathbb{R}^{2N \times N}$ is constructed by stacking the horizontal and vertical finite difference operators, $\mathbf{D} = [\mathbf{D}_x^\top, \mathbf{D}_y^\top]^\top$, taking into account periodic boundary conditions.

The rationale for operating in the gradient domain lies in the statistical properties of natural images. Unlike random noise, natural images typically exhibit piecewise smoothness, meaning that the differences between adjacent pixels are mostly zero or close to zero, except at edges as discussed in Section 2.1.

The denoising task is therefore cast as the minimization of an energy function comprising a quadratic data fidelity term and a regularization term acting on the gradient domain:

$$\hat{\mathbf{x}} = \arg \min_{\mathbf{x}} \left(\frac{1}{2} \|\mathbf{x} - \mathbf{y}\|_2^2 + \lambda H_u(\mathbf{z}) \right), \quad (7.3)$$

where $\mathbf{z} = \mathbf{D}\mathbf{x}$ represents the image gradients (difference coefficients), and $\lambda > 0$ balances noise removal and structure preservation. This formulation promotes sparsity and structural consistency by suppressing the randomness introduced by noise, thereby restoring the low-entropy characteristic of the natural gradient distribution.

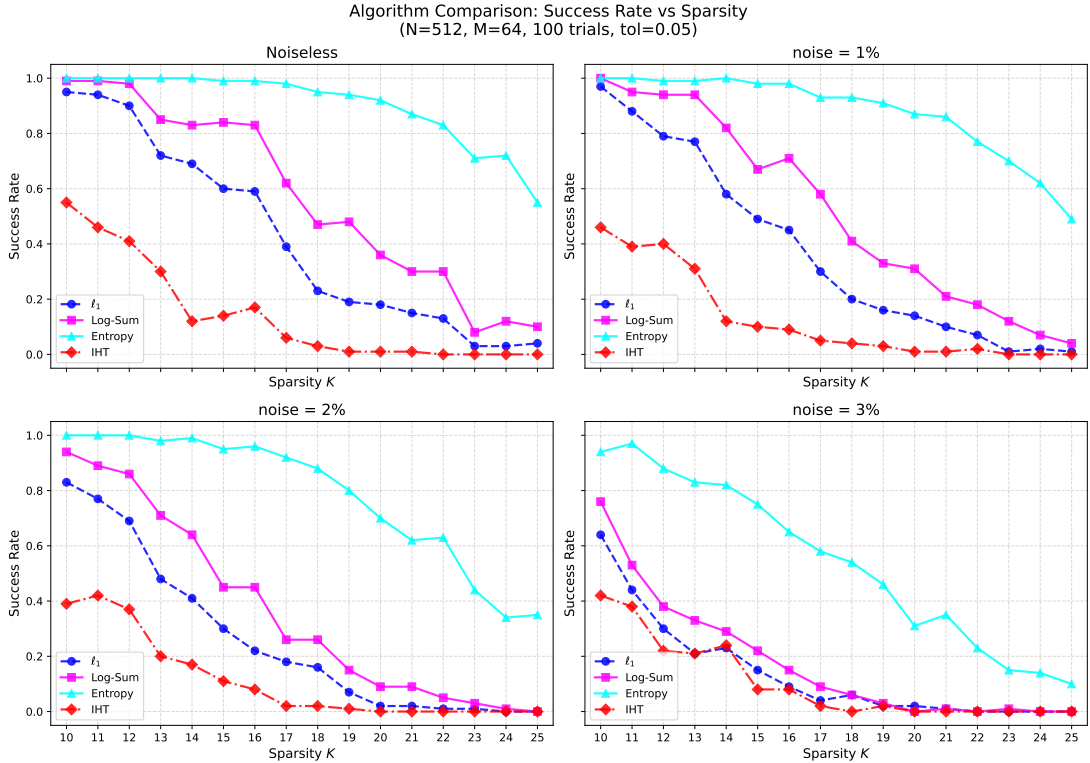


Figure 8: Empirical recovery success rate versus sparsity level for different noise levels ($\eta \in \{0.01, 0.02, 0.03\}$). A trial is counted as successful if $\text{Err}(\hat{\mathbf{x}}) \leq 0.05$. Under the correlated Gaussian sensing model considered here, the proposed entropy regularizer achieves higher success rates across a broader range of sparsity levels, and its performance degrades more gradually as noise increases compared with ℓ_0 , ℓ_1 , and log-sum baselines.

We evaluate the proposed model on standard test images (128×128) corrupted by additive White Gaussian Noise (AWGN) with $\sigma = 0.05$. We compare our proposed entropy regularization with two well-established gradient-domain regularizers: the standard Total Variation (TV) approach [Rudin et al. \(1992\)](#), which applies an ℓ_1 norm on the discrete gradients \mathbf{D} , and a non-convex Log-Sum penalty [Candès et al. \(2008\)](#), which is tailored to further enhance gradient sparsity. For our proposed method, we utilize the unnormalized metric entropy on gradients and set the scaling constant to $C = 1$, justified by the fact that the maximum possible difference between adjacent pixels in a normalized image is exactly 1. It should be emphasized that while the denoised image $\hat{\mathbf{x}}$ is fundamentally obtained by minimizing the formulated energy function, metrics such as Peak Signal-to-Noise Ratio (PSNR) and the Structural Similarity Index Measure (SSIM) [Wang et al. \(2004\)](#) serve strictly as independent criteria to assess the final reconstruction quality. To ensure a fair comparison, the hyperparameter λ for all methods was tuned via a logarithmic grid search (10^{-4} to 10^2) to yield its optimal PSNR performance.

PERFORMANCE EVALUATION

Reconstruction quality is assessed quantitatively using PSNR and SSIM. Let \mathbf{x} be the ground-truth clean image and $\hat{\mathbf{x}}$ be the denoised image. The PSNR evaluates the pixel-level fidelity and is defined as:

$$\text{PSNR}(\hat{\mathbf{x}}, \mathbf{x}) = 10 \log_{10} \left(\frac{\text{MAX}_I^2}{\frac{1}{N} \|\hat{\mathbf{x}} - \mathbf{x}\|_2^2} \right), \quad (7.4)$$

where $\text{MAX}_I = 1.0$ for normalized images.

The SSIM Wang et al. (2004) evaluates the visual impact of luminance, contrast, and structure similarities, which is formulated as:

$$\text{SSIM}(\hat{\mathbf{x}}, \mathbf{x}) = \frac{(2\mu_{\hat{\mathbf{x}}}\mu_{\mathbf{x}} + C_1)(2\sigma_{\hat{\mathbf{x}}\mathbf{x}} + C_2)}{(\mu_{\hat{\mathbf{x}}}^2 + \mu_{\mathbf{x}}^2 + C_1)(\sigma_{\hat{\mathbf{x}}}^2 + \sigma_{\mathbf{x}}^2 + C_2)}, \quad (7.5)$$

where μ and σ^2 denote the mean and variance of the respective images, $\sigma_{\hat{\mathbf{x}}\mathbf{x}}$ is the covariance between $\hat{\mathbf{x}}$ and \mathbf{x} , and C_1, C_2 are small positive constants used to stabilize the division.

Table 1 summarizes the quantitative results on the standard test images.

Table 1: Quantitative comparison of denoising algorithms (PSNR / SSIM). Best values are boldfaced.

Method	Cameraman		Synthetic		Horse	
	PSNR	SSIM	PSNR	SSIM	PSNR	SSIM
TV	28.37	0.8198	32.62	0.2585	29.05	0.8140
Log-Sum	30.93	0.8375	34.01	0.2670	32.22	0.8249
Entropy	31.25	0.8760	34.14	0.2725	32.02	0.8295

Evaluation under AWGN ($\sigma = 0.05$). The proposed Entropy regularizer consistently achieves the highest SSIM across all test images and the best PSNR on *Cameraman* and *Synthetic*. For the *Horse* image, it maintains superior structural preservation with a PSNR highly competitive to the Log-Sum baseline, demonstrating a more favorable overall trade-off.

The quantitative results highlight the strong performance of the proposed entropy-based regularization. Across all three test images, the Entropy model achieves the best PSNR on *Cameraman* (31.25 dB) and *Synthetic* (34.14 dB), and the highest SSIM on both *Horse* (0.8295) and *Synthetic* (0.2725). For the *Horse* image, Entropy attains the best SSIM while its PSNR is only marginally below that of Log-Sum (32.02 dB vs. 32.22 dB), indicating a favorable trade-off between noise suppression and structural fidelity. Overall, these results, together with the visual comparisons, demonstrate that entropy-based regularization provides a more effective sparsity prior than TV and Log-Sum, delivering consistently superior or competitive reconstructions.

Visual comparisons are presented in Figure 9. Standard ℓ_1 regularization can suffer from “cartoon-like” artifacts in smooth regions. In contrast, the entropy regularizer better

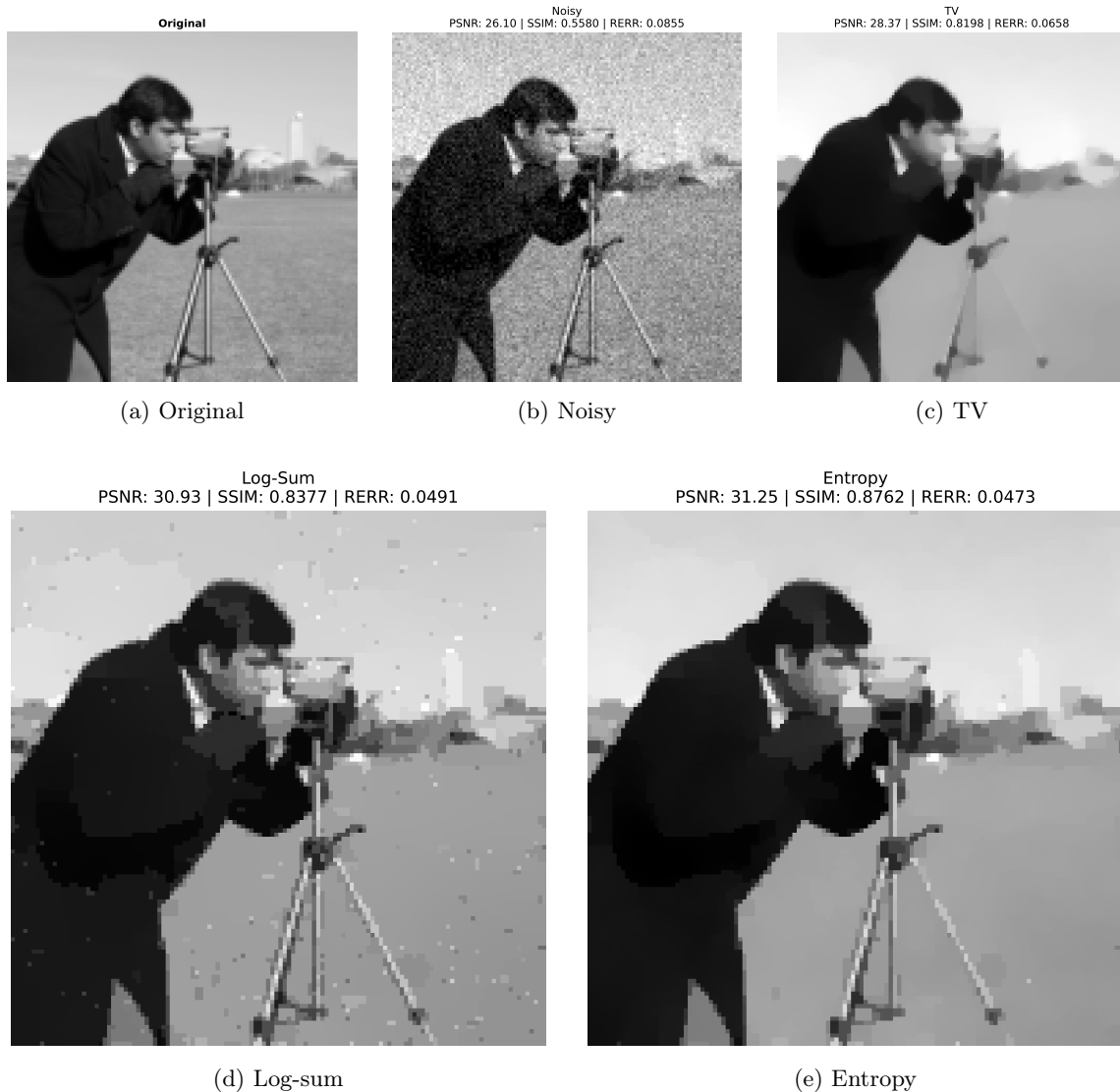


Figure 9: Denoising results on *Cameraman* under AWGN ($\sigma = 0.05$). Compared with TV and Log-sum, the entropy regularizer produces a visually cleaner reconstruction with reduced residual noise while preserving edge transitions and fine structures.

preserves fine edges and geometric structures while suppressing noise artifacts, corroborating the quantitative improvements shown in Table 1.

8 Conclusion and Future Work

In this work, we introduced the effective number of nonzeros (ENZ) as a metric for effective sparsity in underdetermined linear inverse problems. Unlike the classical ℓ_0 pseudo-norm, which indiscriminately counts all nonzeros, ENZ captures the concentration of significant

signal components while naturally attenuating negligible entries. Our numerical experiments confirm that ENZ remains highly stable under small-amplitude perturbations and noise.

The core advantage of ENZ lies in its ability to overcome the limitations of classical Restricted Isometry Property (RIP) analysis. Traditional RIP frameworks rely on a rigid k -sparse assumption. However, real-world solutions inevitably contain numerous small nonzeros due to noise or numerical errors, which destroys the strict k -sparse structure and renders standard RIP conditions overly restrictive. By quantifying effective sparsity through normalized magnitudes rather than discrete counting, ENZ bypasses the rigid k -sparse requirement. It effectively absorbs negligible components, thereby relaxing the stringent limitations of traditional RIP analysis and providing a more robust, practical metric for recovery guarantees.

Future work will proceed in two main directions. Algorithmically, integrating entropy-based regularization with proximal quasi-Newton methods or stochastic optimization could improve computational scalability. Analytically, extending the ENZ framework to structured settings—such as group or hierarchical sparsity—will expand its utility for more complex inverse problems.

Acknowledgment This work was supported by the General Program of the National Natural Science Foundation of China (NSFC) under No. 12571326.

References

- Jacob Abernethy and Alexander Rakhlin. Beating the adaptive bandit with high probability. In *2009 Information Theory and Applications Workshop*, pages 280–289. IEEE, 2009.
- Daniel Alabi, Pravesh K Kothari, Pranay Tankala, Prayaag Venkat, and Fred Zhang. Privately estimating a gaussian: Efficient, robust, and optimal. In *Proceedings of the 55th Annual ACM Symposium on Theory of Computing*, pages 483–496, 2023.
- Amir Beck and Marc Teboulle. A fast iterative shrinkage-thresholding algorithm for linear inverse problems. *SIAM Journal on Imaging Sciences*, 2(1):183–202, 2009.
- Peter J. Bickel, Ya’acov Ritov, and Alexandre B. Tsybakov. Simultaneous analysis of Lasso and Dantzig selector. *The Annals of Statistics*, 37(4):1705–1732, 2009. doi: 10.1214/08-AOS620. URL <https://doi.org/10.1214/08-AOS620>.
- Jeffrey D Blanchard, Coralia Cartis, and Jared Tanner. Compressed sensing: How sharp is the restricted isometry property? *SIAM Review*, 53(1):105–125, 2011.
- Thomas Blumensath and Mike E Davies. Iterative thresholding for sparse approximations. *Journal of Fourier analysis and Applications*, 14(5):629–654, 2008.
- Florentina Bunea, Alexandre Tsybakov, and Marten Wegkamp. Sparsity oracle inequalities for the Lasso. *Electronic Journal of Statistics*, 1(none):169–194, 2007. doi: 10.1214/07-EJS008. URL <https://doi.org/10.1214/07-EJS008>.

- E.J. Candes and T. Tao. Decoding by linear programming. *IEEE Transactions on Information Theory*, 51(12):4203–4215, 2005. doi: 10.1109/TIT.2005.858979.
- Emmanuel J. Candès. The restricted isometry property and its implications for compressed sensing. *Comptes Rendus. Mathématique*, 346(9-10):589–592, 2008. doi: 10.1016/j.crma.2008.03.014. URL <https://www.numdam.org/articles/10.1016/j.crma.2008.03.014/>.
- Emmanuel J Candès and Michael B Wakin. An introduction to compressive sampling. *IEEE Signal Processing Magazine*, 25(2):21–30, 2008.
- Emmanuel J Candès, Justin Romberg, and Terence Tao. Robust uncertainty principles: Exact signal reconstruction from highly incomplete frequency information. *IEEE Transactions on Information Theory*, 52(2):489–509, 2006.
- Emmanuel J Candes, Justin K Romberg, and Terence Tao. Stable signal recovery from incomplete and inaccurate measurements. *Communications on Pure and Applied Mathematics: A Journal Issued by the Courant Institute of Mathematical Sciences*, 59(8):1207–1223, 2006.
- Emmanuel J. Candès, Michael B. Wakin, and Stephen P. Boyd. Enhancing sparsity by reweighted ℓ_1 minimization. *Journal of Fourier Analysis and Applications*, 14(5-6): 877–905, 2008. doi: 10.1007/s00041-008-9045-x. URL <https://link.springer.com/article/10.1007/s00041-008-9045-x>.
- Rick Chartrand and Valentina Staneva. Restricted isometry properties and nonconvex compressive sensing. *Inverse Problems*, 24(3):035020, 2008.
- Scott Shaobing Chen, David L Donoho, and Michael A Saunders. Atomic decomposition by basis pursuit. *SIAM Review*, 43(1):129–159, 2001.
- Thomas M Cover. *Elements of Information Theory*. John Wiley & Sons, 1999.
- David L Donoho. Compressed sensing. *IEEE Transactions on Information Theory*, 52(4): 1289–1306, 2006.
- Jianqing Fan and Runze Li. Variable selection via nonconcave penalized likelihood and its oracle properties. *Journal of the American statistical Association*, 96(456):1348–1360, 2001.
- Simon Foucart and Holger Rauhut. *A Mathematical Introduction to Compressive Sensing. Applied and Numerical Harmonic Analysis*. Birkhäuser, New York, NY, 2013. ISBN 978-0-8176-4947-0. doi: 10.1007/978-0-8176-4948-7.
- Ralph VL Hartley. Transmission of information. *Bell System Technical Journal*, 7(3):535–563, 1928.
- Mark O Hill. Diversity and evenness: a unifying notation and its consequences. *Ecology*, 54(2):427–432, 1973.

- Niall Hurley and Scott Rickard. Comparing measures of sparsity. *IEEE Transactions on Information Theory*, 55(10):4723–4741, 2009.
- Edwin T Jaynes. Information theory and statistical mechanics. *Physical Review*, 106(4):620, 1957.
- Solomon Kullback and Richard A Leibler. On information and sufficiency. *The Annals of Mathematical Statistics*, 22(1):79–86, 1951.
- Miles Lopes. Estimating unknown sparsity in compressed sensing. In *International Conference on Machine Learning*, pages 217–225. PMLR, 2013.
- Nicolai Meinshausen and Bin Yu. Lasso-type recovery of sparse representations for high-dimensional data. *The Annals of Statistics*, 37(1):246–270, 2009. doi: 10.1214/07-AOS582. URL <https://doi.org/10.1214/07-AOS582>.
- Tom Mitchell. Twenty Newsgroups. UCI Machine Learning Repository, 1997. URL <https://archive.ics.uci.edu>. Dataset.
- Balas Kausik Natarajan. Sparse approximate solutions to linear systems. *SIAM journal on computing*, 24(2):227–234, 1995.
- Yaghoub Rahimi, Chao Wang, Hongbo Dong, and Yifei Lou. A scale-invariant approach for sparse signal recovery. *SIAM Journal on Scientific Computing*, 41(6):A3649–A3672, 2019.
- Alfréd Rényi. On measures of entropy and information. In *Proceedings of the fourth Berkeley symposium on Mathematical Statistics and Probability, volume 1: Contributions to the Theory of Statistics*, volume 4, pages 547–562. University of California Press, 1961.
- Olivier Roy and Martin Vetterli. The effective rank: A measure of effective dimensionality. In *2007 15th European Signal Processing Conference*, pages 606–610. IEEE, 2007.
- Leonid I Rudin, Stanley Osher, and Emad Fatemi. Nonlinear total variation based noise removal algorithms. *Physica D: nonlinear phenomena*, 60(1-4):259–268, 1992.
- Claude E Shannon. A mathematical theory of communication. *The Bell System Technical Journal*, 27(3):379–423, 1948.
- Vincent Thibeault, Antoine Allard, and Patrick Desrosiers. The low-rank hypothesis of complex systems. *Nature Physics*, 20(2):294–302, 2024.
- Robert Tibshirani. Regression shrinkage and selection via the lasso. *Journal of the Royal Statistical Society Series B: Statistical Methodology*, 58(1):267–288, 1996.
- Constantino Tsallis. Possible generalization of boltzmann-gibbs statistics. *Journal of statistical physics*, 52(1):479–487, 1988.
- Zhou Wang, Alan C Bovik, Hamid R Sheikh, and Eero P Simoncelli. Image quality assessment: from error visibility to structural similarity. *IEEE transactions on image processing*, 13(4):600–612, 2004.

Yiming Xu, Akil Narayan, Hoang Tran, and Clayton G Webster. Analysis of the ratio of ℓ_1 and ℓ_2 norms in compressed sensing. *Applied and Computational Harmonic Analysis*, 55: 486–511, 2021.

Penghang Yin, Yifei Lou, Qi He, and Jack Xin. Minimization of ℓ_{1-2} for compressed sensing. *SIAM Journal on Scientific Computing*, 37(1):A536–A563, 2015.